Science Advances
AAAS

advances.sciencemag.org/cgi/content/full/6/14/eaay4858/DC1

Supplementary Materials for

ENL initiates multivalent phase separation of the super elongation complex (SEC) in controlling rapid transcriptional activation

Chenghao Guo, Zhuanzhuan Che, Junjie Yue, Peng Xie, Shaohua Hao, Wei Xie, Zhuojuan Luo*, Chengqi Lin*

*Corresponding author. Email: cqlin@seu.edu.cn (C.L.); zjluo@seu.edu.cn (Z.L.)

Published 1 April 2020, *Sci. Adv.* **6**, eaay4858 (2020)
DOI: 10.1126/sciadv.aay4858

This PDF file includes:

Supplementary Figure Legend

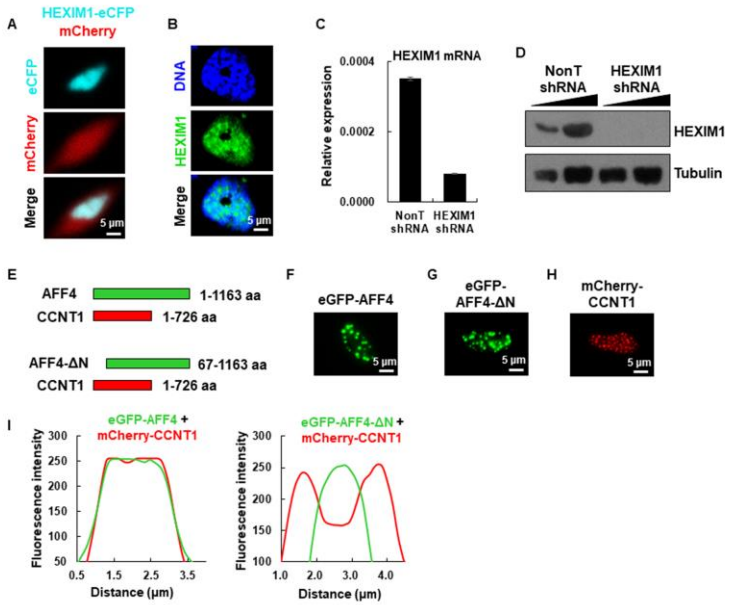

Fig. S1. AFF4, but not HEXIM1, compartmentalizes CCNT1 into phase-separated droplets.

(A) Live cell imaging of HeLa cells co-expressing mCherry and HEXIM1-eCFP. (B) IF imaging of HEXIM1 in HeLa cells. DNA was counterstained using DAPI. (C) RT-qPCR showing the efficiency of the shRNA-mediated HEXIM1 knockdown in HCT 116 cells. Results shown are representative of three biological replicates. Error bars represent standard deviations. (D) Western blot showing the efficiency of the shRNA-mediated HEXIM1 knockdown. β-Tubulin was used as a loading control. (E) Schematic representation of mCherry-CCNT1, eGFP-AFF4 and eGFP-AFF4-ΔN used in Fig. 1G. (F to H) Live cell imaging of HeLa cells expressing eGFP-AFF4 (F), eGFP-AFF4-ΔN (G) and mCherry-CCNT1 (H). (I) Integrated fluorescence intensity distributions versus distance in the multi-channel merged zoomed-in images shown in Fig. 1G. Color lines represent AFF4 (green) and CCNT1 (red) signals, respectively.

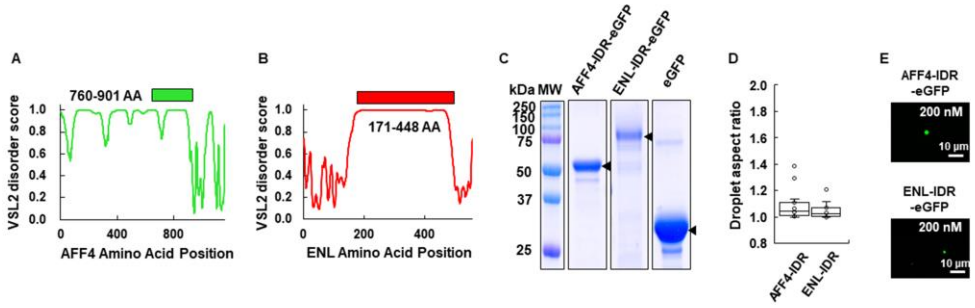

Fig. S2. Purification of recombinant eGFP fused AFF4 and ENL IDRs.

(A and B) Graph plots showing the intrinsic disorder across the entire length of AFF4 (A) and ENL (B) calculated by PONDR (Predictor of Natural Disordered Regions) VSL2 algorithm. The intrinsic scores are shown on the y-axis, and amino acid positions are shown on the x-axis. The scores are assigned between 0 and 1, and the score above 0.5 indicates disorder. The green and red bars represent the selected IDRs under investigation in this study. (C) The AFF4-IDR-eGFP, ENL-IDR-eGFP, and eGFP proteins were purified from recombinant BL21, and analyzed by SDS-PAGE followed by Coomassie blue staining. (D) Box plots showing the aspect ratio of the AFF4-IDR-eGFP and ENL-IDR-eGFP droplets, respectively. Each n>20; error bars represent the distribution between the 90th and 10th percentiles. Results shown are representative of two biological replicates. (E) Fluorescence microscopy images showing the formation of small AFF4-IDR-eGFP and ENL-IDR-eGFP droplets when low concentration (200 nM) of purified fusion proteins were added into the droplet formation buffer containing 50 mM NaCl.

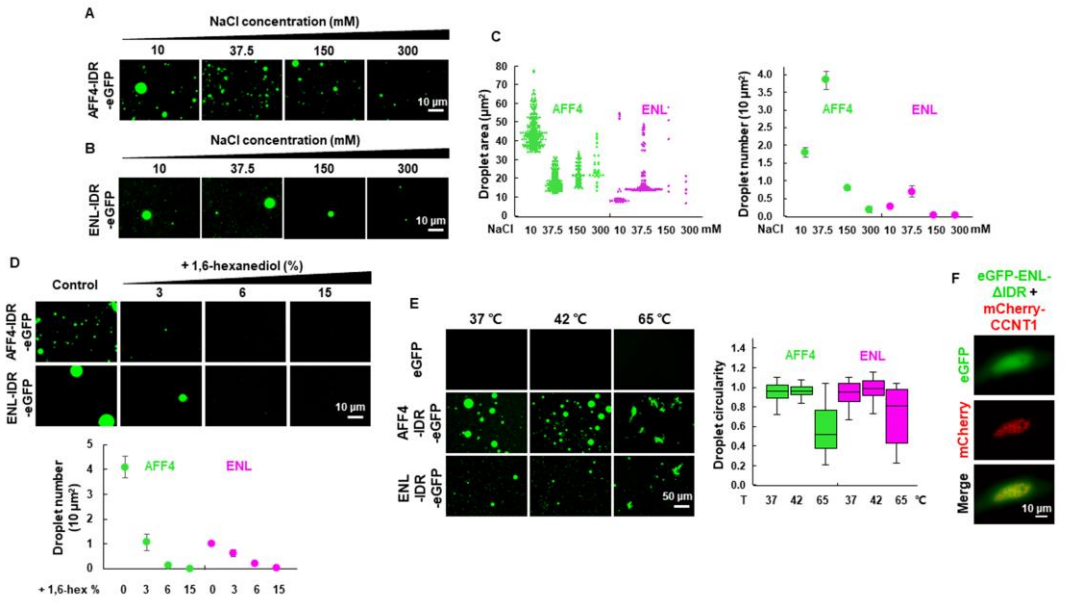

Fig. S3. IDRs of AFF4 and ENL phase-separate *in vitro*.

(A and B) Fluorescence microscopy images showing the formation of the homotypic AFF4-IDR-eGFP (A) and ENL-IDR-eGFP (B) droplets in buffers containing different concentrations of NaCl. 20 μM of purified recombinant proteins were used, and the droplet formation buffer contains 10% PEG-8000. (C) Droplet area (left) and number (right) analyses are also shown for Fig. S3A and S3B. Error bars represent standard deviations. Results are representative of three biological replicates. (D) Fluorescence microscopy images (upper) showing that the homotypic AFF4-IDR-eGFP or ENL-IDR-eGFP droplets are disrupted by 1,6-hexanediol in a dosage dependent manner. 20 μM of purified recombinant proteins were used, and the droplet formation buffer contains 10% PEG-8000 and 50 mM NaCl. Droplet number analyses (lower) are also shown. Error bars represent standard deviations. Results are representative of three biological replicates. (E) Fluorescence microscopy images (left) showing the homotypic AFF4-IDR-eGFP or ENL-IDR-eGFP droplets at different temperature. Purified eGFP was used as a negative control. 20 μM of purified recombinant proteins were used, and the droplet formation buffer contains 10% PEG-8000 and 50 mM NaCl. Droplet Circularity analyses (right) are shown. Error bars represent standard deviations. Results are representative of three biological replicates. (F) Live cell imaging of HeLa cells co-expressing eGFP-ENL-ΔIDR and mCherry-CCNT1.

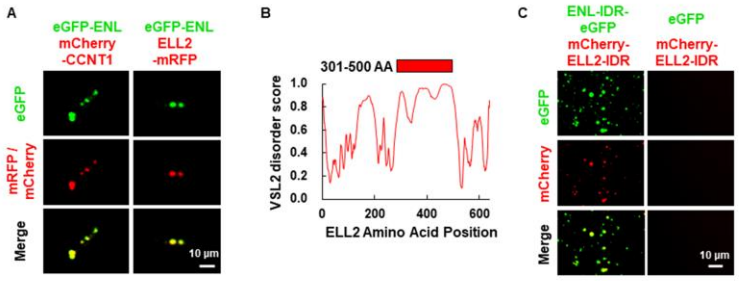

Fig. S4. ELL2 can form heterotypic droplets with ENL.

(A) Live cell imaging of HeLa cells co-expressing eGFP-ENL together with mCherry-CCNT1 or ELL2-mRFP. (B) Graph plots showing the intrinsic disorder region across the entire length of ELL2 calculated by PONDR VSL2 algorithm. The intrinsic scores are shown on the y-axis, and amino acid positions are shown on the x-axis. The scores are assigned between 0 and 1, and the score above 0.5 indicates disorder. The red bar represents the selected IDR under investigation in this study. (C) Fluorescence microscopy images showing that purified mCherry-ELL2-IDR can form heterotypic droplets together with ENL-IDR-eGFP. Purified eGFP was used as a negative control. 20 μM of purified recombinant proteins were used, and the droplet formation buffer contains 10% PEG-8000 and 50 mM NaCl.

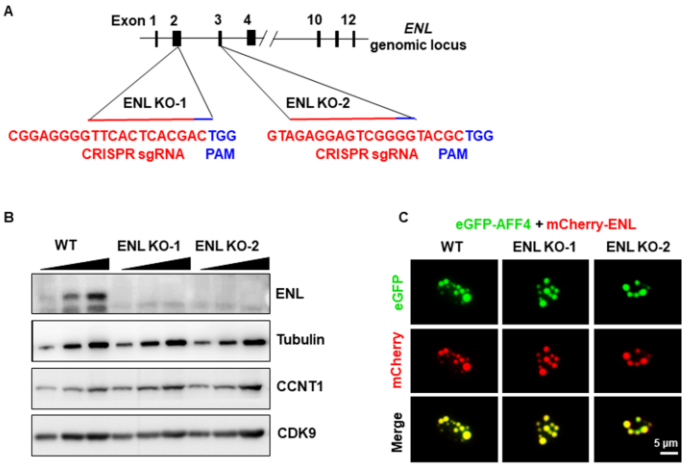

Fig. S5. Generation of ENL knockout HCT 116 cell lines and disruption of AFF4 droplets in ENL knockout cells can be rescued by overexpression of ENL.

(A) Schematic representation of the positions of the 2 sgRNAs used to knock out ENL. (B) Western blot analysis of ENL, CCNT1, and CDK9 in the wild type and ENL knockout HCT 116 cells. β-Tubulin was used as a loading control. (C) Live cell imaging of HCT 116 wild type and ENL knockout cells expressing eGFP-AFF4 and mCherry-ENL.

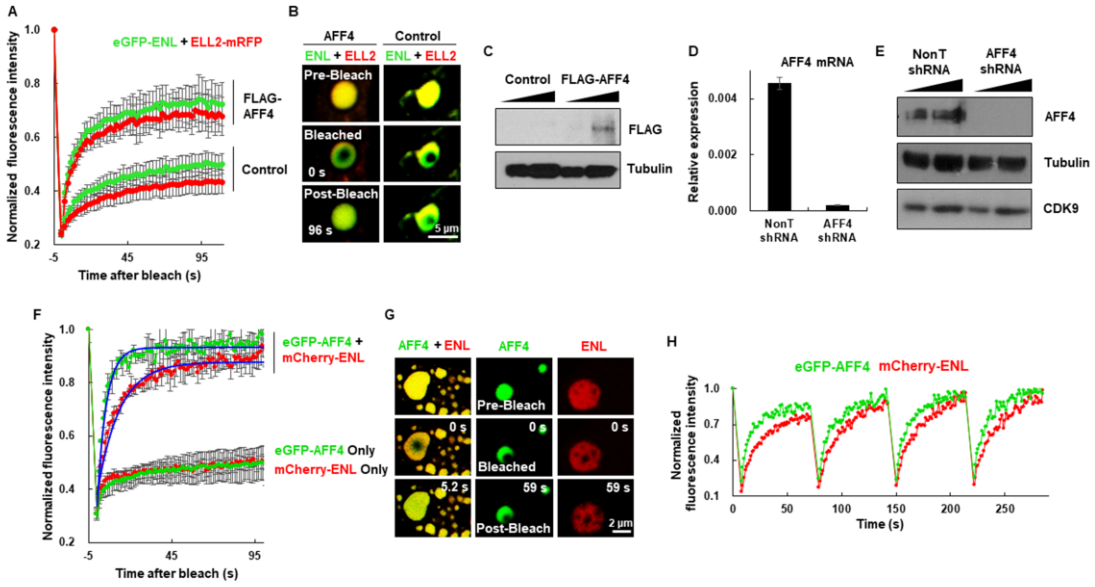

Fig. S6. Both AFF4 and ENL are essential for fluidity of SEC puncta.

(A) Normalized FRAP recovery curves for eGFP-ENL (green) and ELL2-mRFP (red) in the heterotypic droplet in the presence or absence of FLAG-AFF4. The bleaching events occurred at 0 second. Results shown are from six biological replicates. Error bars represent standard deviations. (B) Live cell confocal images showing FRAP of the heterotypic eGFP-ENL and ELL2-mRFP droplet in the presence or absence of FLAG-AFF4. (C) Western blot analysis of FLAG-AFF4 in the control and FLAG-AFF4 overexpressing HeLa cells. β-Tubulin was used as a loading control. (D) RT-qPCR showing the efficiency of the shRNA-mediated AFF4 knockdown in cells. Results shown are representative of three biological replicates. Error bars represent standard deviations. (E) Western blot analysis of AFF4 and CDK9 in the control and AFF4 knockdown cells. β-Tubulin was used as a loading control. (F) Normalized FRAP recovery curves for eGFP-AFF4 (green) and mCherry-ENL (red) in the eGFP-AFF4 homotypic, mCherry-ENL homotypic, and eGFP-AFF4 and mCherry-ENL heterotypic droplets. The bleaching events occurred at 0 second. The nonlinear fitting curve (blue) of normalized fluorescence recovery data is shown. Results shown are from six biological replicates. Error bars represent standard deviations. (G) Live cell confocal images showing the above FRAP events. (H) Normalized FRAP recovery curves for eGFP-AFF4 (green) and mCherry-ENL (red) for 4 rounds of bleach. The first bleaching event occurred at 0 second.

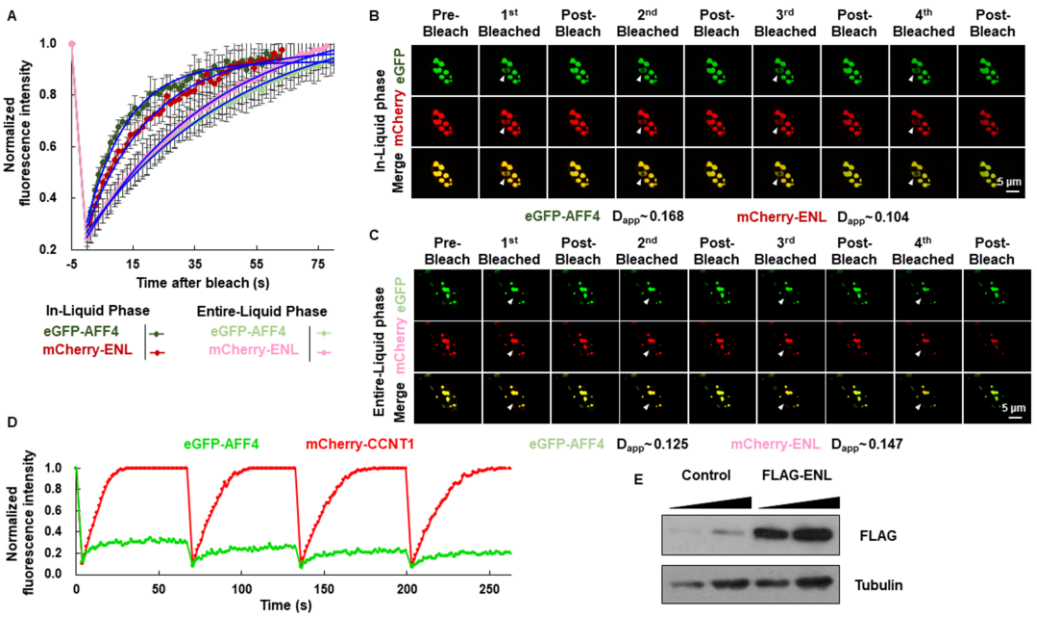

Fig. S7. The ENL and AFF4 heterotypic droplets exhibit fluidity.

(A) Normalized FRAP recovery curves for eGFP-AFF4 (green: in-liquid phase; or reseda: entire-liquid phase) and mCherry-CCNT1 (red: in-liquid phase; or pink: entire-liquid phase) in the eGFP-AFF4 and mCherry-ENL heterotypic droplets. The nonlinear fitting curve (blue) of normalized fluorescence recovery data is shown. Results shown are from six biological replicates. Error bars represent standard deviations. (B and C) Live cell confocal images showing FRAP of the eGFP-AFF4 and mCherry-ENL heterotypic droplets under in-liquid phase (B) and entire-liquid phase (C) conditions. (D) Normalized FRAP recovery curves for eGFP-AFF4 (green) and mCherry-CCNT1 (red) for 4 rounds of bleach. The first bleaching event occurred at 0 second. (E) Western blot analysis of FLAG-ENL in the control and FLAG-ENL overexpressing cells. β-Tubulin was used as a loading control.

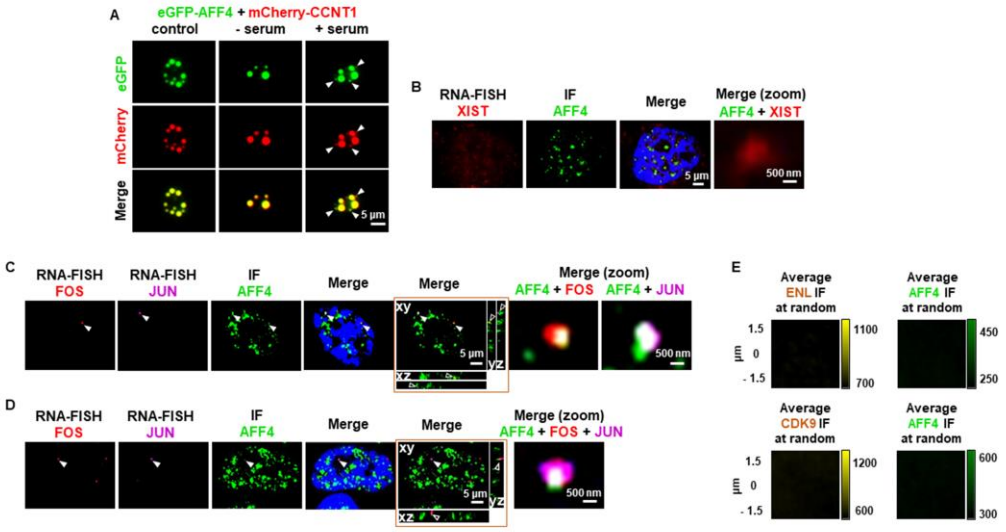

Fig. S8. SEC puncta localizes to immediate response genes in vivo upon serum treatment.

(A) Live cell imaging of HCT 116 cells co-expressing eGFP-AFF4 and mCherry-CCNT1 in the control, serum-starved and serum-treated conditions. The newly formed eGFP-AFF4 and mCherry-CCNT1 heterotypic droplets after serum treatment are indicated by arrows. (B) Confocal imaging of XIST RNA FISH with the concurrent AFF4 IF in HeLa cells in the serum-treated condition. DNA was counterstained using DAPI. A zoomed-in view region is shown. (C-D) Confocal imaging of FOS and JUN FISH with the concurrent AFF4 IF in HeLa cells in the serum-treated condition showing that colocalization of AFF4 puncta, FOS and JUN transcripts. DNA was counterstained using DAPI. A reconstructed 3D merged image is highlighted in yellow box. A zoomed-in view of the white arrow indicated region is shown. (E) Average immunofluorescence signal for ENL or AFF4 centered at randomly selected nuclear positions (upper). Average immunofluorescence signal for CDK9 or AFF4 centered at randomly selected nuclear positions (lower).

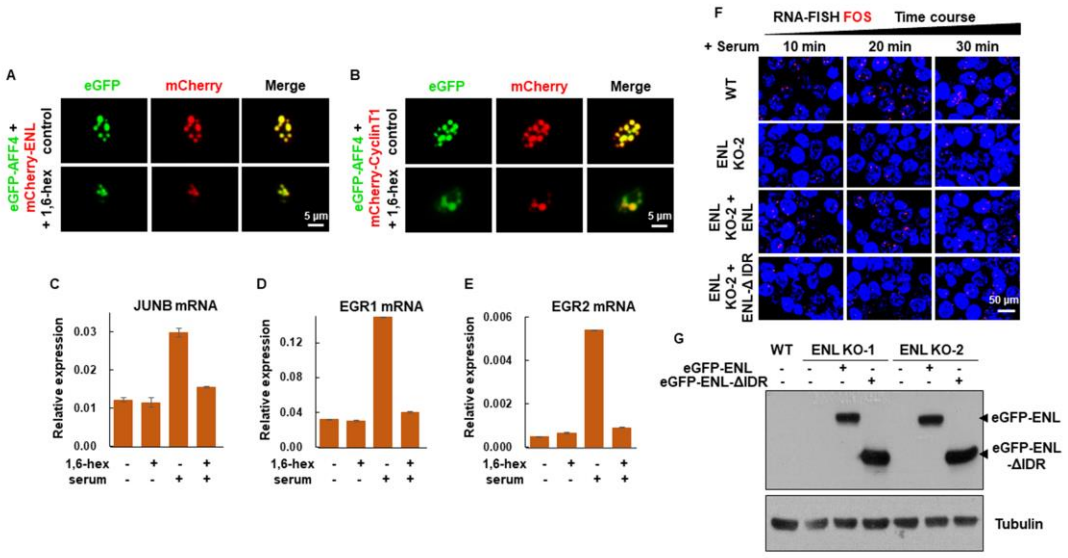

Fig. S9. ENL is required for the rapid induction of FOS gene upon serum treatment.

(A and B) Live cell imaging of HCT 116 cells expressing eGFP-AFF4 with mCherry-ENL (A) or mCherry-CCNT1 (B) before and after 3% 1,6-hexanediol treatment for 30 minutes. (C-E) RT-qPCR showing the RNA levels of JUNB (C), EGR1 (D) and EGR2 (E) under indicated conditions. Results shown are representative of three biological replicates. Error bars represent standard deviations. (F) Confocal imaging of FOS FISH in the wild type and ENL knockout-2 HCT 116 cells after serum stimulation for different time periods. Only wild type ENL, but not the ENL IDR deletion mutant, can rescue FOS transcriptional induction defect caused by ENL knockout. DNA was counterstained using DAPI. (G) Western blot analysis of eGFP-ENL and eGFP-ENL-ΔIDR in the ENL knockout HCT 116 cells. β-Tubulin was used as a loading control.